Geografiska Annaler: Series A, Physical Geography

ISSN: 0435-3676 (Print) 1468-0459 (Online) Journal homepage: http://www.tandfonline.com/loi/tgaa20

Sediments from around the lower younger dryas boundary (se arizona, usa): implications from la-icp-ms multi-element analysis

Alexandre V. Andronikov & Irina E. Andronikova

To cite this article: Alexandre V. Andronikov & Irina E. Andronikova (2016) Sediments from around the lower younger dryas boundary (se arizona, usa): implications from la-icp-ms multi-element analysis, Geografiska Annaler: Series A, Physical Geography, 98:3, 221-236, DOI: 10.1111/geoa.12132

To link to this article: https://doi.org/10.1111/geoa.12132

SEDIMENTS FROM AROUND THE LOWER YOUNGER DRYAS BOUNDARY (SE ARIZONA, USA): IMPLICATIONS FROM LA-ICP-MS MULTI-ELEMENT ANALYSIS

ALEXANDRE V. ANDRONIKOV[1,2] and IRINA E. ANDRONIKOVA[2]

[1]Department of Geosciences, University of Arizona, Tucson, AZ, USA
[2]Lunar and Planetary Laboratory, University of Arizona, Tucson, AZ, USA

Andronikov, A.V., and Andronikova, I.E., 2016. Sediments from around the lower Younger Dryas boundary (SE Arizona, USA): implications from LA-ICP-MS multi-element analysis. *Geografiska Annaler: Series A, Physical Geography*, 98, 221–236. DOI:10.1111/geoa.12132

ABSTRACT. One of the prominent features in sediment sequences formed around the Allerød-Younger Dryas transition (*c*. 12.9–12.8 ka BP) in North America is a dark layer of organic-rich material, i.e. the black mat. The black mat sequences in southeast Arizona contain a thin sandy basal layer corresponding to the lower Younger Dryas boundary. Trace element concentrations in the lower Younger Dryas boundary sediments, in the black mat, in the host sediments, and in charcoal from Western Europe and southeast Arizona were studied using LA-ICP-MS. The black mat samples and samples of the underlying host sediments display compositions similar to the average continental crust, while the sediments from the lower Younger Dryas boundary are enriched in rare earth elements, Ni, and Co whereas Ta, Nb, Zr, and Hf are depleted relative to the rare earth elements. Such a difference in compositions between the lower Younger Dryas boundary sediments and other sediments points to a short enigmatic event, which changed conditions of sedimentation just before the onset of the Younger Dryas cooling. The presence of products of biomass burning of still unknown origin is suggested on the basis of trace element features of sediments from the lower Younger Dryas boundary.

Key words: sediments, trace elements, Younger Dryas

Introduction

The last glacial–interglacial transition in the northern hemisphere ended with the beginning of the cold period known as the Younger Dryas climate oscillation, whose onset is dated at *c*. 12.9–12.8 ka BP (e.g. Peteet 1995; Alley 2000; Björck 2007; Lowe *et al.* 2008; Wittke *et al.* 2013; Kennett *et al.* 2015). This sharp and short (~1200 years; Berger 1990; Peteet 1995; Alley 2000; Friedrich *et al.* 2000; van der Hammen and van Geel 2008) Late Pleistocene cooling event may have resulted in the extinction of megafauna and in the decline of the Clovis prehistoric culture (e.g. Berger 1990; Beck 1996; Anderson *et al.* 2011; Ballenger *et al.* 2011). The Younger Dryas climate change is generally thought to result from an abrupt change of atmospheric and oceanic circulations (e.g. Berger 1990; Teller *et al.* 2002; McManus *et al.* 2004; Brauer *et al.* 2008; Murton *et al.* 2010; Rayburn *et al.* 2011).

One of the prominent features in sedimentary sequences deposited around the Allerød-Younger Dryas transition in North America is the presence of a dark layer of organic-rich material, i.e. the black mat (e.g. Haynes 2007, 2008; Pigati *et al.* 2009, 2012; Ballenger *et al.* 2011; Harris-Parks 2016). Overall, the black mat is a general term that includes, in addition to the dark organic-rich deposits, some Younger Dryas marls and diatomites that are light grey in color (e.g. Haynes 1995). Black layers which are both younger and older than the black mat are also known in North America (Haynes 2007; Pigati *et al.* 2012), but they are not as widely distributed as the Younger Dryas black mat. This black mat is a very reliable stratigraphic marker dating the Allerød-Younger Dryas transition. The major hypotheses on the origin of the black mat suggest that it was formed by either water-transported organic material, or as the result of a heavy deposition of algae in a shallow fresh-water reservoir (see Haynes 2007, 2008 and Harris-Parks 2016 for more references), or in response to periods of spring-fed stream activation when groundwater oxidized the organic material (Quade *et al.* 1998; Harris-Parks 2016). However, the reported presence of charcoal (Haynes 2007), soot, polycyclic aromatic hydrocarbons and glass-like carbon in or around the lower Younger

DOI:10.1111/geoa.12132

Dryas boundary (LYDB) allowed some authors to suggest extensive wildfires and decomposition of charred wood as a response to a short and probably catastrophic event (Firestone *et al.* 2007; Marlon *et al.* 2009; Mahaney *et al.* 2010). On the other hand, some other authors strongly disagree with an idea about a short and dramatic event resulted in conflagration just before the onset of the Younger Dryas climate oscillation. They argue that if wildfires even occurred, those wildfires were not simultaneous as a result of some catastrophic event, but were significantly extended in time (e.g. Pinter *et al.* 2011; van Hoesel *et al.* 2012).

We analyzed sediments from around the Allerød-Younger Dryas transition in the southwestern USA (Arizona; Fig. 1) and a few charcoal samples from W. Europe and from Arizona by the *laser ablation—inductively coupled plasma—mass spectrometry* (*LA-ICP-MS*). This method was chosen because of the high concentration of organic materials in some samples, which could be tough to dissolve during sample preparations for more conventional ICP-MS analysis. In this paper, we discuss what the analyses revealed about the trace element characteristics of the studied samples.

Brief sample descriptions

We studied nine samples collected from around the Allerød-Younger Dryas transition and three samples of the host sediments (both above and below the black mat sequence) from the Late Pleistocene outcrops of Murray Springs (MS samples), and two samples from a drill core from Palominas Arroyo (PLM samples). Additionally, a few charcoal samples were studied because the presence of charcoal is widely discussed in the black mat samples (see Pinter *et al.* 2011 for references).

Murray Springs

The sediments in this locale are thoroughly dated and a stratigraphic sequence is well established (e.g. Haynes 2007, 2008). The sequence consists of two main members: Murray Springs Formation and Lehner Ranch Formation (Haynes 2007). The Murray Springs Formation is represented by the Moson Ranch Member (stratum D_1) of light brown to white calcareous sand; the Sobaipuri Member (stratum D) of olive green mudstone that varies from nearly pure clay to sandy clay; the Coro Marl Member (stratum E) of white marl; the Fry Ranch Member (stratum D_2) of muddy calcareous sand and calcareous sandy mud; the Kendall Ranch Member (stratum E_1) of calcareous sand; and the sporadically present Graveyard Gulch Member (stratum F_1) of light gray to greenish gray medium- to coarse-grained sand (Clovis channel sand). The Lehner Ranch Formation overlays with a discontinue sediments of the Murray Spring Formation and consists of the Clanton Ranch Member (black mat, stratum F_2) of dark organic-rich silty clay; the Earp Member (white marl; stratum F_{2b}) of nearly pure calcite carbonate; and the Donnet Ranch Member (stratum F_3) of eolian sand.

We sampled the following units of the sedimentary sequence from the Murray Springs location:

1. Stratum F_1. Clovis channel sand; from 11 190±180 to 10 840±70 ^{14}C years BP (Haynes 2007).
2. Stratum F_2. Black mat; from 10 760±100 to 10 260±140 ^{14}C years BP (Haynes 2007).
3. Stratum F_{2b}. Earp marl; from 10 250±170 to 9660±150 ^{14}C years BP (Haynes 2007).

The following samples were collected from the Murray Springs area:

1. Samples 2MS10-09 and 3MS10-03 from sediments underlying the black mat are represented by light to greenish medium- to coarse-grained clay-rich sand (Clovis channel sand).
2. Sample 5MS10-02 was collected from a thin (3–5 cm) sandy layer underneath a thicker (35–40 cm) black mat layer. The sandy layer is resting disconformably (Clovis surface) on light-gray sandy silt, i.e. the Clovis channel sands (see Haynes 2007, 2008; Ballenger *et al.* 2011; Fig. 2b). It is possible that the black mat material was initially deposited on a wet clayish surface (cf. Haynes 2007).
3. Samples 4MS10-03 and 4MS10-03A were collected from a thin (5–7 cm) sandy layer underneath a thicker (40–50 cm) black mat layer (a stratigraphic analogue of the sample 5MS10-2). The sandy layer is covering with a disconformity the Clovis channel sands (see Haynes 2007, 2008; Ballenger *et al.* 2011; Fig. 2b).
4. Sample 26MS07 was collected from the lower 0.5 cm of a black mat layer stringer (5–7 cm) within a layer of grayish sandy clay and resting on a thin (3–5 cm) layer of fine-grained grey sand. The stringer of the black mat likely formed in a fresh water environment very soon after the rise of the water table (Haynes 2007; Haynes *et al.* 2010).

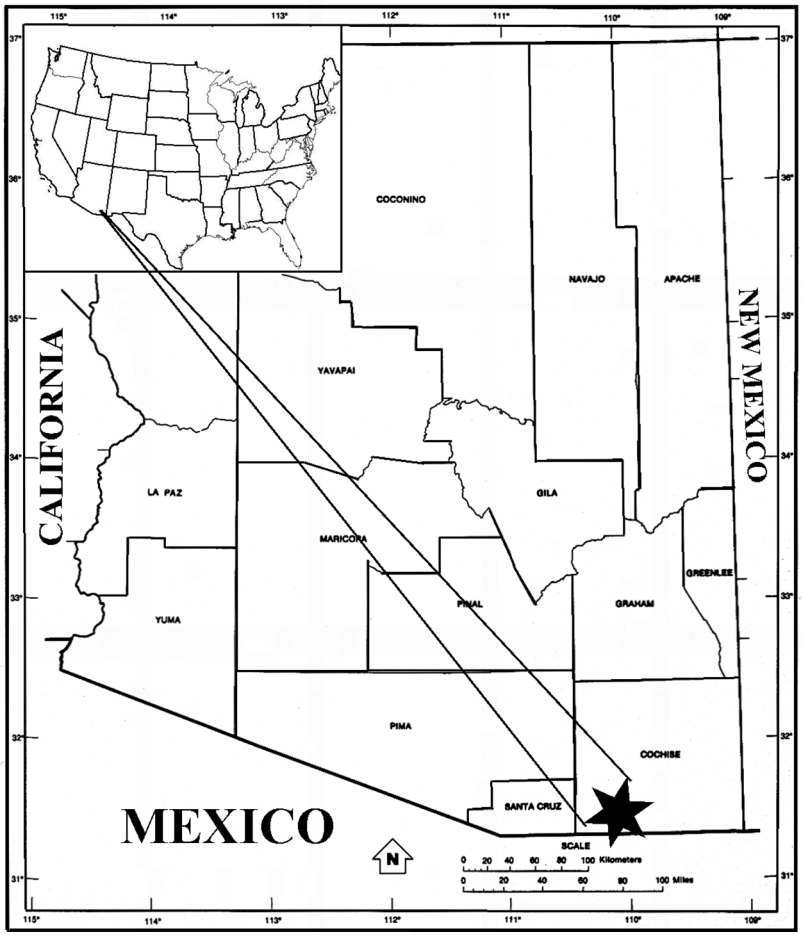

Fig. 1. A map showing the location of Murray Springs and Palominas Arroyo in Arizona, USA (a black star). The location of the sites in the USA is shown as an insert (modified from http://www.lib.utexas.edu/maps/states/arizona.gif).

5. Sample 2MS10-05 was collected from a similar black mat stringer (5–7 cm) within a thick (1 m) layer of grayish marl (Fig. 2a). This occurrence suggests that the black mat accumulated in an aquatic environment, likely in a shallow freshwater pond as in the case of sample 26MS07 (cf. Haynes 2008).
6. Sample 4MS10-04 was collected from the middle of a thick (40–50 cm) black mat layer overlain by the Earp Marl (Fig. 2b). This layer of the black mat was likely exposed to erosion and later, when the water table rose, covered by freshwater sediments.
7. Sample 3MS10-02 was collected from the middle to the upper part of a thick black mat layer (30–40 cm) overlain by the Earp Marl. The upper surface of this black mat layer is uneven, suggesting intense erosion after layer generation and before the water table rose. Therefore, this layer of the black mat was at some stage exposed to erosion, and was later covered by freshwater sediments similar to sample 4MS10-04.
8. Sample 1MS10-01 is from the Earp Marl disconformably overlying a black mat sequence in the Murray Springs location (Fig. 2a, b).

Palominas Arroyo

The sequence in the area consists of stratum IIa represented by channel alluvium with peaty laminations (12.9–11.3 ka BP; Ballenger *et al.* 2011), stratum IIb represented by black organic silty clay and peat (>9.9–9.5 ka BP; Ballenger *et al.* 2011), and a lower part of stratum III represented by alluvium sand (9.5–7.3 ka BP; Ballenger *et al.*

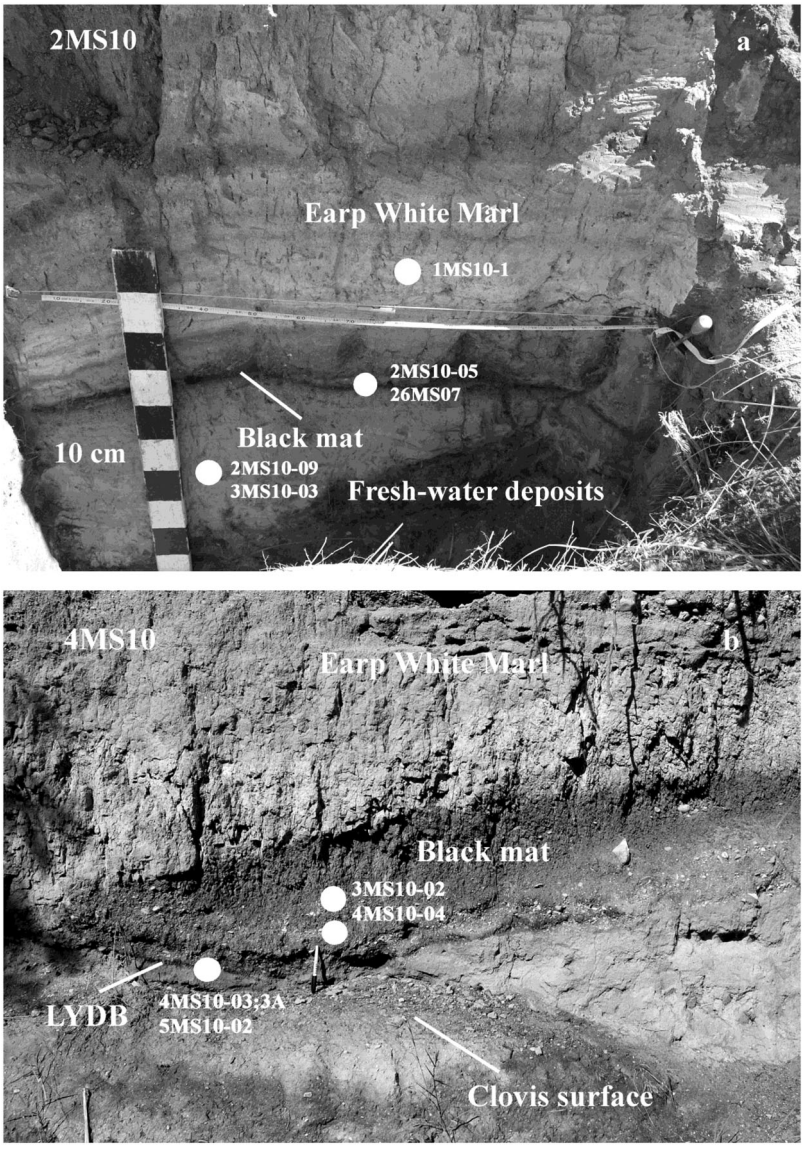

Fig. 2. Examples of black mat occurrences in Murray Springs. (a) Outcrop 2MS10: a thin black mat string is located inside lake deposits (black and white stick is graduated in 10 cm). (b) Outcrop 4MS10: a very thin black layer at the bottom of the black mat corresponds to the LYDB. (a pen stands on the Clovis surface). Location of collected samples is shown (samples from the outcrops 1MS10, 3MS10, 5MS10 and 26MS07 are extrapolated to the shown stratigraphic sections). Figures 2 5 are from the authors' collection.

2011). The lower part of stratum IIa of the sedimentary sequence from the Palominas Arroyo location, contemporaneous with deposition of the Clovis channel sand (F_1) and overlying black mat (F_2) at the Murray Springs (Haynes 2007; Ballenger *et al.* 2011), was sampled.

Sample 1PLM1320-1 is a thick slice cut off the drill core from the depth interval of 13.15–13.20 m (the lower part of this interval corresponding to the lower part of stratum IIb, i.e. the LYDB).

Sample 1PLM1320 is another thick slice cut off the same drill core from the depth interval of 13.15–13.20 m (the upper part of the interval corresponding to the boundary between strata IIa and IIb, i.e. the analogue of the black mat from Murray Springs).

Charcoal

A few charcoal samples were collected from the Late Pleistocene sediments of Western Europe, and from modern wood fires in Arizona.

Sample LUT-CH is paleo-charcoal from the Usselo Horizon deposits (*c*. 13 ka BP; van Hoesel *et al.* 2012) in Lutterzand, the Netherlands. A few small pieces were picked up from a sandy clay-rich matrix.

Sample SWFr is paleo-charcoal from eolian sand of the Allerød- to Younger Dryas-age (Bertran *et al.* 2009) in the Landes area of SW France. A few small pieces were picked up from a matrix of fine- to medium-grained sand.

Samples AzF-A and AzF-B are charcoal fragments from recent wood fires in SE Arizona, USA, collected in Catalina Mountains.

Sample preparations and analytical techniques

Small fragments (0.5–1.0 mm) of black mat samples (8–12 pieces per sample) were handpicked, mounted in epoxy, and polished to achieve a flat surface. For Palominas samples, analyses were conducted *in situ* on slices not mounted in epoxy. Samples of the host sediments and the sediments from the LYDB were pulverized, and the resulting powders were pressed to pellets of 1 cm diameter. Samples of charcoal from sediments of the Netherlands and France were picked up from the host sand, mounted in epoxy and slightly polished to achieve a flat surface. Much bigger fragments of charcoal from modern wood fires in Arizona were slightly polished in order to achieve flat surfaces and then were mounted in modeling clay. The samples were analyzed for trace elements at the Lunar and Planetary Laboratory of the University of Arizona. A CETAC UV Nd:YAG LXS-213 laser coupled with a ThermoFinnigan Element2 ICP-MS was used for analysis. The laser beam was focused onto the sample surface with 200 μm diameter spots, and each sample was analyzed with three spots. During the analytical runs, the laser was operated at 75% maximum energy output (see Table 1 for analytical parameters). The He carrier gas flow was mixed with the Ar gas flow up line of the plasma torch. A NIST SRM-612 silicate glass standard and a pellet made from the International Association of Geoanalysts SdAR-1 material (enhanced river sand; Webb *et al.* 2012) were used as reference materials (Sylvester and Eggins 1997; Jochum *et al.* 2011; Webb *et al.* 2012; Andronikov *et al.* 2013). Analyses were run in the low mass resolution mode of the instrument (i.e. $M/\Delta M_{(5\%)} = 300$). Extended laser analytical time (60–70 sec) provided us with the average bulk composition of the material. Iron57 was used as an internal standard (concentrations of Fe were independently analyzed in solutions by ICP-MS for samples 2MS10-09, 3MS10-03, i.e. sediments underlying the black mat, sample 1MS10-01 from the Earp Marl, and for the International Association of Geoanalysts SdAR-1 material; Webb *et al.* 2012). The laser ablation measurements were based on integrated multi-element time-resolved signals.

Table 1. Instrumental parameters.

Element 2 ICP-MS	
Sample gas flow	1.05 L min^{-1}
Auxiliary gas flow	0.85 L min^{-1}
Coolant gas flow	15.7–16.7 L min^{-1}
Forward power	1200 W
Reflected power	1–3 W
Cones	Al
CETAC LSX-213 Laser ablation unit	
Sample gas flow (Ar)	1.20 L min^{-1}
Carrier gas flow (He)	0.71 L min^{-1}
Laser output energy (100%)	4 mJ pulse^{-1}
Laser repetition rate	20 Hz

One of the challenges in determination of trace elements in natural samples with ICP-MS (especially in the low mass resolution mode) is a danger of interferences of various masses. Among the analyzed set of elements, the *rare earth elements* (*REEs*) are the most easily affected by interferences with oxides (e.g. Zhu *et al* 1997; Haynes *et al.* 2010). That is why, during the preparation stage of the work, we measured the REE both as single charges and as double-charged ions. Our measurements show that there is no real difference in the results except for strong interferences for $^{157}Gd^{+}$ with $^{141}Pr^{16}O$ (e.g. Zhu *et al.* 1997). To avoid these interferences, we used $^{157}Gd^{++}$ ion as a proxy to the element concentration.

Another challenge is the influence of the "matrix effect", i.e. the composition and physical properties of the standards should be as close to those of the analyzed sample as possible (e.g. Jochum *et al.* 2007; Sylvester 2008). To overcome the influence of the "matrix effect", we used two references: one is NIST612 glass standard (Sylvester and Eggins 1997; Jochum *et al.* 2011), and the other is a pellet made from the pulverized International Association of Geoanalysts SdAR-1 material (with physical properties and composition close to those of the analyzed samples; Webb *et al.* 2012). Repeated analyses of the NIST612 standard and the

Table 2. Results of cross-analyses of the applied reference materials.

	LOD*	SdAR-1 Webb *et al.* (2012)	NIST-612 Jochum *et al.* (2011)	Composition of SdAR-1 after NIST-612	2σ	Composition of NIST-612 after SdAR-1	2σ
No. of analyses				12		12	
(ppm)							
P	4	698	46.6	724	107	43.8	6.4
Cr	0.8	92.7	36.4	160	15.2	38.5	3.7
Mn	0.5	5405	38.7	5860	383	38.0	2.7
Fe	60	32 375	51.0	31 245	1550	55.0	8.0
Co	1	10.71	35.5	11.4	0.68	36.4	2.1
Ni	0.5	40.80	38.8	41.4	2.1	37.5	1.8
Y	0.22	40.90	38.3	36.6	2.3	38.7	2.2
Zr	0.25	352.8	37.9	348	19.1	38.3	2.4
Nb	0.05	34.70	38.9	37.5	2.2	40.1	2.4
La	0.15	58.25	36.0	59.5	2.9	35.8	1.8
Ce	0.05	110.9	38.4	102.3	5.3	39.3	1.9
Pr	0.03	12.55	37.9	13.6	0.69	37.6	2.0
Nd	0.2	46.08	35.5	45.4	1.9	35.5	1.4
Sm	0.07	8.525	37.7	9.2	0.44	37.3	2.0
Eu	0.05	1.338	35.6	1.29	0.06	36.6	1.7
Gd	0.3	7.500	37.3	8.86	0.64	38.4	2.7
Tb	0.03	1.213	37.6	1.30	0.06	37.7	1.6
Dy	0.1	7.315	35.5	7.56	0.47	35.8	2.2
Ho	0.04	1.480	38.3	1.55	0.12	38.2	2.9
Er	0.15	4.326	38.0	4.45	0.28	38.2	2.2
Tm	0.02	0.662	36.8	0.656	0.04	36.8	1.8
Yb	0.07	4.280	39.2	4.18	0.22	39.0	1.9
Lu	0.02	0.669	37.0	0.650	0.04	37.3	2.2
Hf	0.04	n.d.	36.7	3.71	0.20	n.d.	
Ta	0.01	2.202	37.6	2.72	0.14	37.2	1.8
W	0.07	10.29	38.0	11.1	0.71	38.2	2.2
Th	0.01	17.97	37.79	19.3	0.81	37.5	1.4
U	0.01	4.277	37.38	5.70	0.35	37.0	2.1

*LOD, limit of detection (ppm).
n.d., no data available.
The following isotopes were monitored during the analytical runs: ^{31}P, ^{52}Cr, ^{55}Mn, ^{57}Fe, ^{59}Co, ^{60}Ni, ^{139}La, ^{140}Ce, ^{141}Pr, ^{143}Nd, ^{147}Sm, ^{153}Eu, ^{157}Gd^{++}, ^{159}Tb, ^{163}Dy, ^{165}Ho, ^{166}Er, ^{169}Tm, ^{172}Yb, ^{175}Lu, ^{178}Hf, ^{181}Ta, ^{182}W, ^{232}Th, and ^{238}U.

International Association of Geoanalysts SdAR-1 material (after every three runs of the unknown samples) ensured that all results are consistent and comparable. Cross-determinations of composition of the reference materials (Table 2) showed that the laser ablation technique provides high-quality results for most trace elements. Because there is no reliable reference material for trace element concentrations in charcoal, all information given below on the composition of charcoal samples should be considered preliminary. Nevertheless, since we are interested only in the behavior of trace elements relative to each other for the purposes of the present study, the results obtained for the charcoal samples are sufficient and are considered in detail in the "Discussion".

Results

Analytical results of the studied samples are summarized in Tables 3 and 4, and shown in Figs 3–5.

Black mat

On an average continental crust-normalized diagram (Fig. 4), all black mat samples display very similar trace element patterns, which are comparable to those for the average continental crust (Wedepohl 1995). Slightly lower normalized values of Zr, Hf, Ta, and Nb compared with the REEs are observed on the spider diagrams. Peaks at U for samples 26MS07, 2MS10-05, and 1PLM1320 (a stratigraphic analogue of the

Table 3. Average trace element composition of samples from Murray Springs and Palominas Arroyo.

Sample			2MS10−05	3MS10−02	4MS10−03	4MS10−03A	4MS10−04
No. of samples			11	8	4	5	12
Note	LOD*	2σ (%)	Black mat	Black mat	LYDB	LYDB	Black mat
Location			Murray Springs				
(ppm)							
Fe	60	5	30 114	30 230	27 851	28 210	29 916
Co	1	6	14.35	10.99	26.97	15.54	15.62
Ni	0.5	5	43.90	36.72	92.19	52.95	33.58
Y	0.22	6	43.37	56.65	1230	417.6	30.60
Zr	0.25	6	111.3	153.4	126.1	220.4	112.2
Nb	0.05	6	18.28	17.01	17.94	27.79	19.97
La	0.15	5	74.91	74.81	537.3	206.6	120.7
Ce	0.05	5	67.91	71.01	302.7	120.9	70.27
Pr	0.03	5	11.26	9.798	67.82	32.95	7.887
Nd	0.2	4	44.64	40.68	336.8	145.6	38.85
Sm	0.07	5	9.387	8.708	83.64	32.62	6.776
Eu	0.05	5	2.032	1.708	17.55	7.425	1.269
Gd	0.3	7	6.324	8.358	101.6	38.75	6.157
Tb	0.03	4	0.765	1.174	14.84	5.501	0.731
Dy	0.1	6	8.210	7.451	107.5	39.23	5.681
Ho	0.04	8	1.731	1.607	24.82	9.065	1.202
Er	0.15	6	5.028	4.858	73.85	27.45	3.339
Tm	0.02	5	0.705	0.691	9.890	3.643	0.827
Yb	0.07	5	4.801	5.098	70.10	27.26	4.121
Lu	0.02	6	0.695	0.695	7.981	3.215	0.517
Hf	0.04	5	3.455	4.224	3.680	5.995	3.156
Ta	0.01	5	1.534	1.398	1.415	2.072	1.568
W	0.07	6	8.943	8.398	9.341	9.863	7.687
Th	0.01	4	15.28	14.13	27.52	19.97	14.14
U	0.01	6	20.16	3.568	3.587	4.530	2.738

Sample No.	5MS10−02	26MS07	1MS10−01	2MS10−09	3MS10−03	1PLM1320	1PLM1320−1
of samples	10	12	7	4	7	6	6
Note	LYDB	Black mat	Earp Marl	Underlying sediments		Black mat	LYDB−BM
Location			Murray Springs			Palominas Arroyo	
(ppm)							
Fe	25 521	36 924	3133	28 815	29 911	128 132	95 977
Co	18.24	n.d.	1.512	7.068	7.271	26.02	78.79
Ni	53.36	n.d.	10.08	20.30	18.08	43.11	87.90
Y	229.1	46.94	3.438	34.85	31.01	48.39	112.8
Zr	183.6	199.9	5.172	246.6	260.6	212.4	312.4
Nb	22.95	23.15	0.496	23.62	21.26	23.98	38.37
La	212.0	519.3	4.321	145.6	88.31	86.30	266.2
Ce	157.4	72.62	3.831	57.89	60.21	103.0	267.9
Pr	27.50	9.371	0.463	8.471	6.796	11.17	25.43
Nd	120.3	38.76	1.786	33.85	26.86	43.52	100.4
Sm	27.37	8.295	0.370	7.282	5.676	9.443	22.34
Eu	5.405	1.582	0.108	1.487	1.139	1.966	4.638
Gd	26.69	7.624	0.352	7.040	6.154	9.327	21.55
Tb	3.602	1.086	0.057	0.897	0.729	1.243	2.848
Dy	24.09	7.115	0.370	5.756	4.762	7.801	18.10
Ho	5.213	1.498	0.084	1.184	1.019	1.614	3.645
Er	15.55	4.563	0.277	3.637	3.220	4.992	10.76
Tm	2.181	0.665	0.059	0.554	0.504	0.717	1.539
Yb	17.47	4.854	0.271	4.232	3.740	5.272	11.09
Lu	1.978	0.652	0.041	0.584	0.516	0.733	1.505
Hf	5.018	5.767	0.135	6.217	6.914	5.985	9.043
Ta	1.817	1.742	0.039	1.712	1.551	1.876	2.887
W	10.53	n.d.	0.501	6.714	6.287	6.216	8.718
Th	21.83	23.11	0.670	15.73	12.25	20.29	36.14
U	4.639	20.14	6.775	8.472	4.056	5.180	11.12

*LOD, limit of detection (ppm).

n.d., the element is not determined.

The following isotopes were monitored during the analytical runs: ^{57}Fe, ^{59}Co, ^{60}Ni, ^{139}La, ^{140}Ce, ^{141}Pr, ^{143}Nd, ^{147}Sm, ^{153}Eu, ^{157}Gd^{++}, ^{159}Tb, ^{163}Dy, ^{165}Ho, ^{166}Er, ^{169}Tm, ^{172}Yb, ^{175}Lu, ^{178}Hf, ^{181}Ta, ^{182}W, ^{232}Th and ^{238}U.

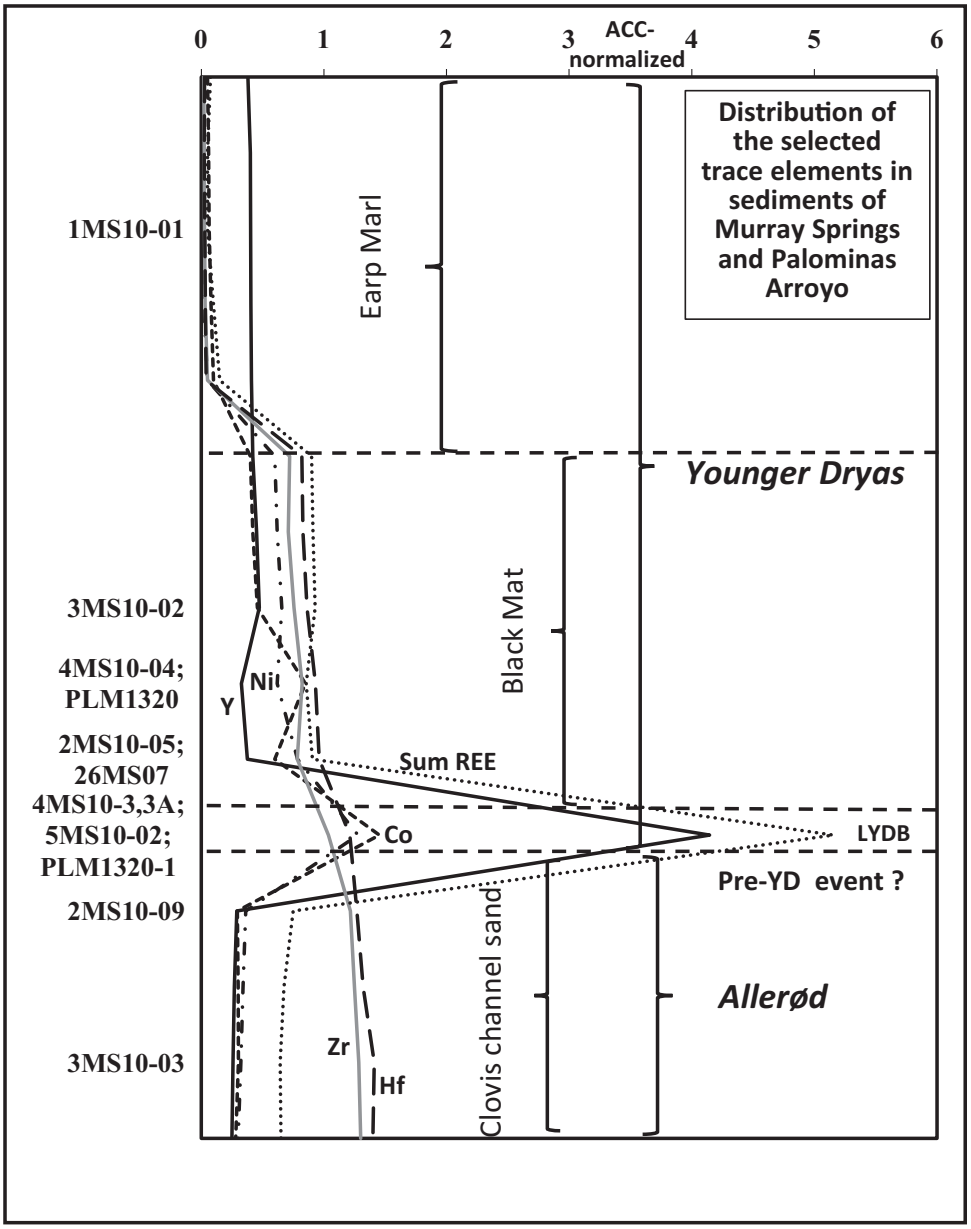

Fig. 3. Schematic distribution of the selected trace elements across the studied part of the sedimentary sequence of Murray Springs and Palominas Arroyo areas. Trace element concentrations are normalized to the average continental crust or ACC (normalizing values are after Wedepohl 1995). Yttrium is given as Y/ACC/5 for the sake of the scale. "Sum REE" is average continental crust-normalized REE values divided in two for the sake of the scale. Dashed black lines mark stratigraphic levels corresponding to the sampled lithologic units (not in the scale); see text for more details. Approximate relative position of the collected samples is given on the left (see Fig. 2 for more details).

Table 4. Chemical composition of paleocharcoal from Lutterzand (the Netherlands), Landes (SW France) and modern charcoal from Arizona (SW USA).

Sample name			LUT-CH	SWFr	AzF-A	AzF-B
Location			Lutterzand	SW France	Arizona	
No. of samples			3	2	3	4
	LOD*	2σ (%)				
(ppm)						
P	4	15	1136	1717	326.2	67.89
Cr	0.8	10	234.6	333.3	6.294	7.597
Mn	0.5	7	31.88	369.1	130.9	31.18
Co	0.2	8	2.544	17.17	1.030	0.232
Ni	0.2	8	16.31	99.23	1.144	0.370
Y	0.01	5	300.0	180.1	11.50	2.942
Zr	0.01	6	173.9	45.80	5.621	2.470
Nb	0.01	6	10.57	5.146	0.971	0.384
La	0.01	10	430.7	1647	47.48	9.930
Ce	0.01	8	385.3	392.9	7.727	1.667
Pr	0.01	7	34.11	63.72	2.069	1.077
Nd	0.01	7	159.4	247.5	6.863	3.212
Sm	0.01	7	40.98	46.83	1.606	0.576
Eu	0.01	7	8.763	10.21	0.438	0.154
Gd	0.05	6	66.15	41.77	6.100	1.505
Tb	0.01	6	8.227	5.236	0.424	0.115
Dy	0.01	7	42.77	28.91	1.360	0.387
Ho	0.01	6	8.509	5.302	0.218	0.074
Er	0.01	8	22.87	13.41	0.806	0.171
Tm	0.01	7	3.028	1.818	0.142	0.026
Yb	0.01	6	18.47	10.19	0.701	0.140
Lu	0.01	7	2.577	1.237	0.077	0.014
Hf	0.01	7	4.640	1.203	0.150	0.048
Ta	0.01	8	1.000	0.375	0.041	0.020
W	0.01	8	1.089	0.720	0.017	0.013
Th	0.01	5	18.05	34.12	0.843	0.219
U	0.01	7	5.287	8.045	0.193	0.075

*LOD, limit of detection (ppm).
The following isotopes were monitored during the analytical runs: ^{31}P, ^{52}Cr, ^{55}Mn, ^{57}Fe, ^{59}Co, ^{60}Ni, ^{89}Y, ^{90}Zr, ^{93}Nb, ^{139}La, ^{140}Ce, ^{141}Pr, ^{143}Nd, ^{147}Sm, ^{153}Eu, ^{157}Gd^{++}, ^{159}Tb, ^{163}Dy, ^{165}Ho, ^{166}Er, ^{169}Tm, ^{172}Yb, ^{175}Lu, ^{178}Hf, ^{181}Ta, ^{182}W, ^{232}Th, and ^{238}U.

black mat) are distinctly pronounced. Elevated concentrations of U are typical for both the black mat samples and the underlying Clovis channel sands (lake/pond sediments; Haynes 2007; Pigati *et al.* 2009, 2012). Uranium is very mobile in aqueous environments, and elevated concentrations in water-formed sediments are known elsewhere (e.g. Tremaine *et al.* 1981). The black mat samples affected by erosion processes are 2–3× lower in U concentrations than the samples with no evidence of erosion processes, which is consistent with the high mobility of the element.

It is notable that concentrations of W in the black mat samples are high (7.5–9 ppm, i.e. 7.5–9× average continental crust), though they are not different from those concentrations in the underlying sediments (Table 3) suggesting a similar source of W for the considered samples. Since W-rich deposits are well known throughout southeast Arizona (e.g. Dale *et al.* 1960), W-rich material could be transported from its original location to places of its present-day accumulation.

LYDB sediments

Samples 4MS10-03, 4MS10-03A, and 5MS10-02, from a thin sandy layer (which could represent the LYDB; West *et al.* 2007) underneath the black mat in Murray Springs area, are distinct because of their strong REE and Y enrichments (>10× average continental crust; Fig. 3), and deep troughs at Zr-Hf (2–3× average continental crust) and (less pronounced) at Ta-Nb relative to the REE. High REE abundances in Younger Dryas microspherules were reported by LeCompte *et al.* (2012), but were not observed in such spherules by Andronikov *et al.* (2016). The sample 1PLM1320-1 from Palominas Arroyo displays trace element patterns that are

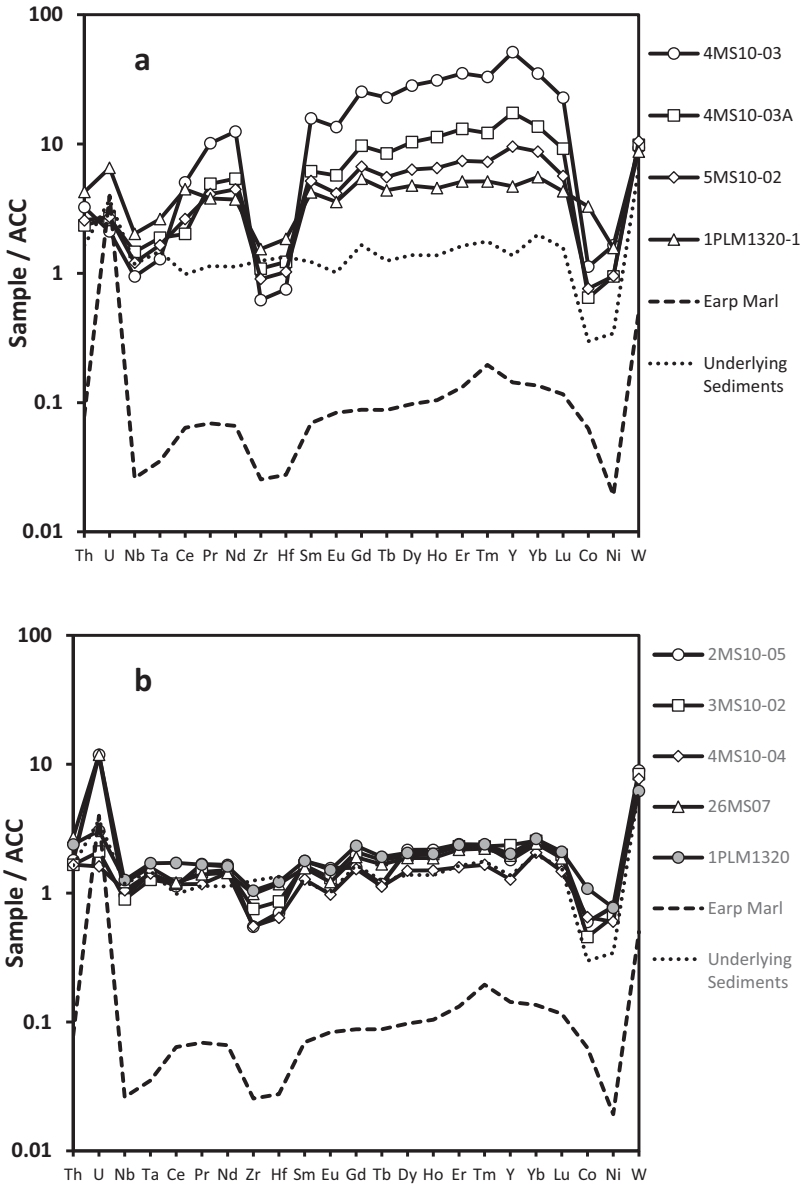

Fig. 4. Average continental crust (ACC)-normalized trace element distribution diagrams. (a) LYDB samples (see text for details). (b) Black mat samples (see text for details) (normalizing values are after Wedepohl 1995). Trace element distributions for Earp Marl (overlaying the black mat) and for sediments underlying the black mat are given for comparison.

similar to those in the Murray Springs LYDB sediments, but the features are not as strongly pronounced (Fig. 4). Concentrations of W are high in the LYDB samples (9–10.5× average continental crust) as is typical for most of the analyzed sediments. It is very notable that concentrations of such siderophile elements as Ni and Co are 1.5–3× higher in the LYDB sediments than in the overlying black mat, and up to 3–5× higher than in the underlying sediments (Clovis channel sands) (Table 3; Fig. 3). Sample 4MS10-3A (and the sample 5MS10-2) from the upper part of the thin LYDB sandy layer shows concentrations of such elements as Ni, Co, REE, and Y to be slightly lower than

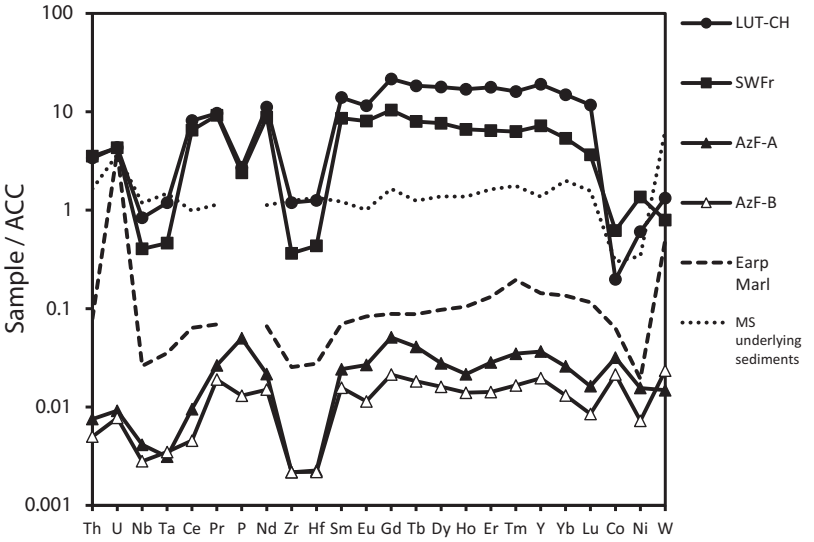

Fig. 5. Average continental crust (ACC)-normalized trace element diagram for Late Pleistocene charcoal samples from the Netherlands and southwest France, and modern charcoal samples from southeast Arizona (normalizing values are after Wedepohl 1995). Characteristic troughs at Nb-Ta, Zr-Hf, and Ti are distinctly observed for the analyzed samples (see text for more details). Trace element distributions for Earp Marl (overlaying the black mat) and for sediments underlying the black mat are given for comparison.

in sample 4MS10-3 from the lowermost part of the same layer.

Host sediments

Concentrations of trace elements in sediments under- and overlying the black mat sequence are very different. The underlying Clovis channel sands display overall trace element concentrations around the average continental crust values (Fig. 4), although concentrations of W are much higher (6–6.5× average continental crust). The Earp Marl overlying the black mat sequence displays very low overall concentrations of trace elements (0.1× average continental crust), except for U (up to 5× average continental crust). Since U is very mobile in aqueous environments, it is not unexpected that its concentrations are high in various aqueous sediments. On the spider diagram (Fig. 4), Zr, Hf, Ta, and Nb display slightly lower concentrations than other analyzed trace elements.

Charcoal

The paleo-charcoal fragments display high concentrations of the REEs (interestingly, Y is either only slightly elevated relative to the REE concentrations or not elevated at all), whereas most other trace elements are characterized by much lower concentrations (Table 4), resulting in deep troughs at Zr-Hf and Ta-Nb on the ACC-normalized spider diagram (Fig. 5). Modern charcoal samples display a similar type of trace-element distribution, but with much lower concentrations of all trace elements (Table 4; Fig. 5).

Discussion

Chemical characteristics of the studied samples suggest that after the uneventful Late Allerød time (sediments are characterized by trace element concentrations close to average continental crust), a sudden short event might have taken place just before the onset of the Younger Dryas cooling 12.9–12.8 ka BP. As a result, the geochemical signatures of the sediments changed. This change is clearly pronounced in the difference between the chemical compositions of the material from the LYDB (both from Murray Springs and from Palominas Arroyo) and all other studied sediments (Fig. 3). One of the most prominent trace element features observed for the LYDB samples is elevated concentrations of the REE (and Y) (cf. LeCompte *et al.* 2012) accompanied by deep troughs at Ta-Nb and Zr-Hf on spider diagrams (Fig. 4). On the other hand, samples from the black mat and its temporal analogues display smooth and almost unfractionated patterns, with trace element concentrations similar to those in the ACC, and only with slightly pronounced depressions at Zr-Hf and

Ta-Nb (Fig. 4). Such distribution of trace elements is also typical for the Clovis channel sands and Earp Marl (Fig. 4).

This characteristic distribution of the trace elements in the LYDB sediments requires special consideration. Observations by Haynes (2007) on the composition of organic matter from the black mat in Murray Springs showed that the samples reflect wood- and alga-related origins. Algae throve on the nutrient-rich ash and cinder, generating dark organic-rich strings in the host clay-rich sand (Fig. 2a). The ash and cinder were produced by wood burning, and may have been delivered to water reservoirs both as airborne particles immediately after the burning occurred (i.e. during the time of sediments of the LYDB accumulation), and later as water streams eroded deposits containing products of burning (i.e. during the time of the black mat formation). Importantly, not only products of wood burning, but also polycyclic aromatic hydrocarbons and glass-like carbon were reported in sediments from around the LYDB elsewhere including from Murray Springs (e.g. Firestone *et al.* 2007; Marlon *et al.* 2009; Mahaney *et al.* 2010). However, such reports encountered strong criticism from some researchers who explain the dark color of some sediment units not by the presence of charcoal or preserved organics, but by clay content and mineralogy (e.g. Pinter *et al.* 2011). Overall, the opponents argue that if wildfires even occurred, they were not simultaneous, but significantly extended in time, and the charcoal does not concentrate along the LYDB, but is scattered across the extended sedimentary sequence (e.g. van Hoesel *et al.* 2012). Therefore, there is still no agreement on the issue.

In order to have a geochemical basis to argue about a possible presence of such products of biomass burning as charcoal in sediments, we analyzed fragments of charcoal from recent wood fires in Arizona, and paleo-charcoal from the Usselo Horizon deposits (*c*. 13 ka BP; van Hoesel *et al.* 2012) in Lutterzand of the Netherlands and from eolian sands of the Allerød to Younger Dryas age (a temporal analogue of the Usselo Horizon; Bertran *et al.* 2009) in the Landes area of southwest France. Although the paleo-charcoal particles are macroscopically distinct from their sand matrix, their trace-element compositions can be influenced by submicroscopic admixture of sediments or by post-depositional adsorption/diffusion processes. The matrix inclusions can be identified and removed from the signal by the spatially resolved LA-ICP-MS technique. We controlled for the possible post-depositional chemical changes by comparing the paleo-charcoal trace-element concentrations with those of charcoal fragments from a modern wood fire that occurred in Arizona a few years ago. Characteristically, all analyzed charcoal samples display elevated REE concentrations with respect to other trace elements, resulting in deep troughs at Zr-Hf and Ta-Nb on average continental crust-normalized spider diagrams (Fig. 5). Overall, the modern charcoal samples display much lower concentrations of trace elements than the paleo-charcoal samples, but the relative distribution patterns of both paleo-charcoal and modern charcoal samples are similar (Table 4; Fig. 5). It is very notable and interesting that the trace-element distribution in the charcoal samples is similar in most features to that displayed by the LYDB sediments (Fig. 4). Although we did not encounter charcoal fragments in the LYDB sediments, the observed similarities in trace-element distributions of both charcoal samples (especially paleo-charcoal samples) and the LYDB sediments are consistent with the presence of charcoal particles (microscopic?) in the LYDB sediments. On the other hand, it is notable that, in spite of the presence of ash and cinder in the black mat deposits (Haynes 2007, 2008), the analyzed black mat samples do not display trace element distribution patterns similar to those for the LYDB sediments. Therefore, it is appropriate to suggest that if the microscopic charcoal fragments are responsible for the described trace element features, such fragments are present only in the LYDB sediments, but not in the black mat (cf. Harris-Parks 2016). Such microscopic fragments, according to geochemical characteristics, are not present in the analyzed samples of the Clovis channel sand either.

It is known that wetter conditions during the Allerød could result in the existence of many dead trees, i.e. abundant fuel for wildfires during earlier stages of the Younger Dryas (Hoek and Bohncke 2002). If this fuel had ignited, it would have resulted in extensive biomass burning, and abundant charcoal fragments might have been produced and deposited, in particular, during deposition of the LYDB sediments (i.e., *c*. 12.9 ka BP). Overall, biomass burning could be due to both the fires induced by various solely terrestrial causes and meteoritic impact (either global or local; cf. Artemieva and Morgan 2009), and we do not have solid evidence yet toward one or another cause. Since we can only tentatively link Ta, Nb, Zr, and Hf depletion, and the REE enrichment with the

conflagrations, these features remain enigmatic and require further investigation.

Another feature displayed by the LYDB sediments is elevated (though not extremely high) concentrations of Ni and Co relative to those in both underlying Clovis channel sands and the overlying black mat (Fig. 3). Those elements are generally not present in high amounts in aqueous sediments (the average continental crust concentrations are 56 ppm and 24 ppm, respectively; Wedepohl 1995), and a sharp and short-term increase in concentrations raises suspicion about addition of an unusual component to the sediments. Since there are no Ni- and Co-rich deposits in the region, which deposits could be responsible for the generation of large amounts of a Ni- and Co-rich component for the LYDB sediments, the source for such a component must have been something other than Ni- and Co-bearing ore deposits. One of the plausible culprits is a meteoritic component added to the sediments. It is known that both Ni and Co (mostly Ni, although Co as well, to a lesser extent) are present in meteorites in much higher concentrations than in most terrestrial sediments: Ni, 1% in chondrites and up to 10% in iron meteorites; Co, 500 ppm in chondrites and up to 0.5% in iron meteorites (e.g. Anders and Grevesse 1989; Haack and Scott 1993; Petaev and Jacobsen 2004). It could be suggested, therefore, that the Ni- and Co-rich component might have been delivered to the LYDB sediments with extraterrestrial material during some short event (e.g. as a result of meteoritic impact/explosion). However, this is not the only possible scenario because both Ni and Co easily complex with organic substances (e.g. Hartland *et al.* 2014), and the sediments could then be enriched in Ni and Co this way as well. Therefore, the presence of a meteoritic component in the LYDB sediments suggested on the basis of geochemical features still remains a subject for discussion.

Conclusions

The distributions of trace elements in samples from around the LYDB in the southwest USA point to a sharp change in conditions of sedimentation just before the onset of the Younger Dryas cooling event (*c*. 12.9–12.8 ka BP). Although most studied sediments do not display any specific geochemical features, some sediments display geochemical features that cannot be explained by the intrinsic characteristics alone. The material displaying unusual trace element characteristics is represented by a thin sandy layer (the LYDB sediments) at the very base of the black mat sequence. The LYDB sediments are characterized by elevated concentrations of REE and troughs at Zr-Hf and Ta-Nb on average continental crust-normalized diagrams. A similar but more strongly pronounced distribution is displayed by the charcoal samples. Therefore, we tentatively relate such a "charcoal-like" trace element distribution in the LYDB sediments to the presence of products of biomass burning. Overall, biomass burning could be due to either the fires induced by various solely terrestrial causes (both natural and artificial) or by meteoritic impact (either global or local) or both. However, the possibility that the observed elevated REEs and Zr-Hf and Ta-Nb troughs are related to factors other than biomass burning should not be ruled out, and their presence requires further detailed investigation to examine the likelihood of burning and any other potential causes. In addition to the "charcoal-like" distribution of the trace elements, the LYDB sediments display some enrichment in Ni and Co. We do not rule out a possible presence of a meteoritic component in the sediments, but the geochemical features observed could also be due to the interaction of Ni and Co with organic substances (although in this case there is no obvious explanation why Ni and Co are enriched only in the thin sandy layer beneath the black mat). The material from the black mat (overlying the LYDB sediments) does not show any unusual geochemical features, and was formed by terrestrial processes in response to a climatic change during the Younger Dryas. It is quite possible that some short and dramatic event took place just before the onset of the Younger Dryas climate oscillation, but, as it was emphasized in Haynes *et al.* (2010), an understanding of what happened at *c*. 12.9–12.8 ka BP requires further research.

Acknowledgements

The authors thank D.S. Lauretta for provided opportunity to work in the LPL cosmochemistry laboratory. R.J. Maxwell and J.S.M. Ballenger are thanked for help with fieldworks. J.S.M. Ballenger is also thanked for providing us with the Palominas samples. P. Bertran is thanked for providing us with samples from SW France. We thank J.S.M. Ballenger, C.V. Haynes Jr, A. van Hoesel, W.Z. Hoek, M. Drury, E. Rudnickaitė, D. Subetto, and C. Verbruggen for the fruitful discussion of the obtained results. Two anonymous reviewers are thanked for reading the earlier version of the manuscript, and for invaluable comments and suggestions. I. Fay Barton is thanked for checking

English. This study was supported in part by the NAI International Collaboration Fund for AVA.

Alexandre V. Andronikov, Department of Geosciences, University of Arizona, 1040 E. 4th Street, Tucson, AZ 85721, USA
Email: alexandronikov@gmail.com

Irina E. Andronikova, Lunar and Planetary Laboratory, University of Arizona, 1415 N. 6th Ave., Tucson, AZ 85705, USA
Email: irandron@yahoo.com

References

Alley, R.B., 2000. The Younger Dryas cold interval as viewed from central Greenland. *Quaternary Science Review*, 19, 213–226.

Anders, E. and Grevesse, N., 1989. Abundances of the elements: meteoritic and solar. *Geochimica et Cosmochimica Acta*, 53, 197–214.

Anderson, D.G., Goodyear, A.C., Kennett, J. and West, A., 2011. Multiple lines of evidence for a possible human decline during the early Younger Dryas. *Quaternary International*, 242, 570–583.

Andronikov, A.V., Andronikov, I.E., Loehn, C.W., Lafuente, B., Ballenger, J.A.M., Crawford, G.T. and Lauretta, D.S., 2016. Implications from chemical, structural and mineralogical studies of magnetic microspherules from around the lower Younger Dryas boundary (New Mexico, USA). *Geografiska Annaler: Part A, Physical Geography*. doi: 10/1111/geoa.12122

Andronikov, A.V., Lauretta, D.S., Connolly, Jr H.C. and Andronikova, I.E., 2013. Determination of trace-element bulk composition of equilibrated ordinary chondrite meteorite samples by LA-ICP-MS using various reference materials. 44th Lunar and Planetary Science Conferences. *Lunar and Planetary Institute Contribution*, No. 1719, 1603.

Artemieva, N. and Morgan, J., 2009. Modeling the formation of the K-Pg boundary layer. *Icarus*, 201, 768–780.

Ballenger, J.S.M., Holliday, V.T., Kowler, A.L., Reitze, W.T., Prasciunas, M.M., Miller, D.S. and Windingstad, J.D., 2011. Evidence for Younger Dryas global climate oscillation and human response in the American Southwest. *Quaternary International*, 242, 502–519.

Beck, M.W., 1996. On discerning the cause of Late Pleistocene Megafaunal Extinctions. *Paleobiology*, 22, 91–103.

Berger, W.H., 1990. The Younger Dryas cold spell – a quest for causes. *Global and Planetary Change*, 3, 219–237.

Bertran, P., Allenet, G., Ge, T., Naughton, F., Poirier, P. and Sanchez Goni, M.F., 2009. Coversand and Pleistocene paleosols in the Landes region, southwestern France. *Journal of Quaternary Science*, 24, 259–269.

Björck, S., 2007. Younger Dryas oscillation, global evidence. In: Scott, A.E. (ed.), *Encyclopedia of Quaternary Science*. Oxford, Elsevier. 1983–1995.

Brauer, A., Haug, G.H., Dulski, P., Sigman, D.M. and Negendank, J.F.W., 2008. An abrupt wind shift in Western Europe at the onset of the Younger Dryas cold period. *Nature Geoscience*, 1, 520–523.

Dale, V.B., Stewart, L.A. and McKinney, W.A., 1960. Tungsten deposits of Cochise, Pima and Sanata Cruz Counties, Ariz. *Bureau of Mines Report of Investigations*, 5650, 139 pp.

Firestone, R.B., West, A., Kennett, J.P., Bunch, T.E., Revay, Z.S., Schultz, P.H., Belgya, T., Kennett, D.J., Erlandson, J.M., Dickenson, O.J., Goodyear, A.C., Harris, R.S., Howard, G.A., Kloosterman, J.B., Lechler, P., Mayewski, P.A., Montgomery, J., Poreda, R., Darrah, T., Que Hee, S.S., Smith, A.R., Stich, A., Topping, W., Wittke, J.H. and Wolbach, W.S., 2007. Evidence for an extraterrestrial impact 12,900 years ago that contributed to the megafaunal extinctions at the Younger Dryas cooling. *Proceedings of the National Academy of Science*, 104, 16016–16021.

Friedrich, M., Kromer, B., Spurk, M., Hofmann, J. and Kaiser, K.F., 2000. Paleo-environment and radiocarbon calibration as derived from Lateglacial/Early Holocene tree-ring chronologies. *Quaternary International*, 61, 27–39.

Haack, H. and Scott, E.R.D., 1993. Chemical fractionations in Group IIIAB iron meteorites: Origin by dendritic crystallization of an asteroidal core. *Geochimica et Cosmochimica Acta*, 57, 3457–3472.

Harris-Parks, E., 2016. The micromorphology of Younger Dryas-aged black mats from Nevada, Arizona, Texas and New Mexico. *Quaternary Research*. doi: 10.1016/j.yqres.2015.11.005

Hartland, A., Fairchild, I.J., Muller, W. and Dominguez-Villar, D., 2014. Preservation of NOM-metal complexes in a modern hyperalkaline stalagmite: implications for speleothem trace element geochemistry. *Geochimica et Cosmochimica Acta*, 128, 29–43.

Haynes, C.V., Jr, 1995. Geochronology of paleoenvironmental change, Clovis type site, Blackwater Draw, New Mexico. *Geoarchaeology*, 10, 317–388.

Haynes, C.V., Jr, 2007. Nature and origin of the black mat, Stratum F_2. In: Haynes, C.V., Jr and Huckell, B.B. (eds.), *Murray Springs. A Clovis Site with Multiple Activity Areas in the San Pedro Valley, Arizona Anthropological Papers of the University of Arizona*, 71, 240–249.

Haynes, C.V., Jr, 2008. Younger Dryas "black mat" and the Rancholabrean termination in North America. *Proceedings of the National Academy of Sciences USA*, 105, 6520–6525.

Haynes, C.V., Jr, Boerner, J., Domanik, K., Lauretta, D., Ballenger, J. and Goreva, J., 2010. The Murray Spring Clovis site, Pleistocene extinction, and the question of extraterrestrial impact. *Proceedings of the National Academy of Sciences USA*, 107, 4010–4015.

Hoek, W.Z. and Bohncke, S.J.P., 2002. Climatic and environmental events over the Last Termination, as recorded in The Netherlands: A review. *Netherlands Journal of Geosciences*, 81, 123–137.

Jochum, K.P., Stoll, B., Herwig, K. and Willbold, M., 2007. Validation of LA-ICP-MS trace element analysis of geological glasses using a new solid-state 193 nm Nd:YAG laser and matrix-match calibration. *Journal of Analytical and Atomic Spectrometry*, 22, 112–121.

Jochum, K.P., Weis, U., Stoll, B., Kuzmin, D., Yang, Q., Raczek, I., Jacob, D.E., Stracke, A., Birbaum, K., Frick, D.A., Günther, D. and Enzweiler, J., 2011. Determination of reference values for NIST SRM

610–617 glasses following ISO guidelines. *Geostandards and Geoanalytical Research*, 35, 397–429.

Kennett, J.P., Kennett, D.J., Culleton, B.J., Tortosa, J.E.A., Bischoff, J.L., Bunch, T.E., Daniel, I.R., Jr, Erlandson, J.M., Ferraro, D., Firestone, R.B., Goodyear, A.C., Israde-Alcantara, I., Johnson, J.R., Jorda Pardo, J.F., Kimbel, D.R., LeCompte, M.A., Lopinot, N.H., Mahaney, W.C., Moore, A.M.T., Ray, J.H., Stafford, T.W., Jr, Tankersley, K.B., Wittke, J.H., Wolbach, W.S. and West, A., 2015. Bayesian chronologic analyses consistent with synchronous age of 12,835-12,735 Cal B.P. for Younger Dryas boundary on four continents. *Proceedings of the National Academy of Sciences USA*, 112, E4344–E4353.

LeCompte, M.A., Goodyear, A.C., Demitroff, M.N., Batchelor, D., Vogel, E.K., Mooney, C., Rock, B.N. and Seidel, A.W., 2012. Independent evaluation of conflicting microspherule results from different investigations of the Younger Dryas impact hypothesis. *Proceedings of the National Academy of Sciences USA*, 109, E2960–E2969.

Lowe, J.J., Rasmussen, S.O., Björck, S., Hoek, W.Z., Steffensen, J.P., Walker, M.J.C., Yu, Z.C. and INTIMATE group, 2008. Synchronisation of palaeoenvironmental events in the North Atlantic region during the Last Termination: a revised protocol recommended by the INTIMATE group. *Quaternary Science Reviews*, 27, 6–17.

Mahaney, W.C., Kalm, V., Krinsley, D.H., Tricart, P., Schwartz, S., Dohm, J., Kim, K.J., Kapran, B., Milner, M.W., Beukens, R., Boccia, S., Hancock, R.G.V., Hart, K.M. and Kelleher, B., 2010. Evidence from the northwestern Venezuelan Andes for extraterrestrial impact: The black mat enigma. *Geomorphology*, 116, 48–57.

Marlon, J.R., Bartlein, P.J., Walsh, M.K., Harrison, S.P., Brown, K.J., Edwards, M.E., Higuera, P.E., Power, M.J., Anderson, R.S., Briles, C., Brunelle, A., Carcaillet, C., Daniels, M., Hu, F.S., Lavoi, M., Long, C., Minckley, T., Richard, P.J.H., Scott, A.C., Shafer, D.S., Tinner, W., Umbanhowar, C.E., Jr, and Whitlock, C., 2009. Wildfire responses to abrupt climate change in North America. *Proceedings of the National Academy of Sciences USA*, 106, 2519–2524.

McManus, J.F., Francois, R., Gherardi, J.M., Keigwin, L.D. and Brown-Legar, S., 2004. Collapse and rapid resumption of Atlantic meridional circulation linked to deglacial climate changes. *Nature*, 428, 834–837.

Murton, J.B., Bateman, M.D., Dallimore, S.R., Teller, J.T. and Yang, Z., 2010. Identification of Younger Dryas outburst flood path from Lake Agassiz to the Arctic Ocean. *Nature*, 464, 740–743.

Petaev, M.I. and Jacobsen, S.B., 2004.Differentiation of metal-rich meteoritic parent bodies: I– Measurement of PGEs, Re, Mo, W and Au in meteoritic Fe-Ni metal. *Meteoritics and Planetary Science*, 39, 1685–1697.

Peteet, D., 1995. Global Younger Dryas? *Quaternary International*, 28, 93–104.

Pigati, J.S., Bright, J.E., Shanahan, T.M. and Mahan, S.M., 2009. Late Pleistocene paleohydrology near the boundary of the Sonoran and Chihuahuan Desert, southeastern Arizona, USA. *Quaternary Science Reviews*, 28, 286–230.

Pigati, J.S., Latorre, C., Rech, J.A., Betancourt, J.L., Martinez, K.E. and Buddahn J.R., 2012. Accumulation of impact markers in desert wetlands and implication for the Younger Dryas impact hypothesis. *Proceedings of the National Academy of Sciences USA*, 109, 7208–7212.

Pinter, N., Scott, A.C., Daulton, T.L., Podoll, A., Koeberl, C., Anderson, R.S. and Ishman, S.E., 2011. The Younger Dryas impact hypothesis: a requiem. *Earth Science Reviews*, 106, 247–264.

Quade, J., Forester, R.M., Pratt, W.L. and Carter C., 1998. Black mats, spring-fed streams, and Late-Glacial-age recharge in the Southern Great Basin. *Quaternary Research*, 49, 129–148.

Rayburn, J.A., Cronin, T.M., Franzi, D.A., Knuepfer, P.L.K. and Willard, D.A., 2011. Timing and duration of North American glacial lake discharges and the Younger Dryas climate reversal. *Quaternary Research*, 75, 541–551.

Sylvester, P.J., 2008. Matrix effects in laser ablation-ICP-MS. *Mineralogic Association of Canada Short Course*, 40, 67–78.

Sylvester, P.J. and Eggins, S.M., 1997. Analysis of Re, Au, Pd, Pt and Rh in NIST glass certified reference materials and natural basalt glasses by laser ablation ICP-MS. *Geostandards Newsletter*, 21, 215–229.

Teller, J.T., Leverington, D.W. and Mann, J.D., 2002. Freshwater outbursts to the ocean from glacial Lake Agassiz and their role in climate change during the last deglaciation. *Quaternary Science Reviews*, 21, 879–887.

Tremaine, P.R., Chen, J.D., Wallace, G.J. and Boivin, W.A., 1981. Solubility of uranium (IV) oxide in alkaline aqueous solutions to 300ºC. *Journal of Solution Chemistry*, 10, 221–230.

Van der Hammen, T. and Van Geel, B., 2008. Charcoal in soils of the Allerød-Younger Dryas transition were the result of natural fires and not necessarily the effect of an extraterrestrial impact. *Netherlands Journal of Geosciences*, 87, 359–361.

Van Hoesel, A., Hoek, W., Braatbaard, F., Van der Plicht, H., Pennock, J.M. and Drury, M.R., 2012. Nanodiamonds and wildfire evidence in the Usselo horizon postdate the Allerød-Younger Dryas boundary. *Proceedings of the National Academy of Sciences USA*, 109, 7648–7653.

Webb, P.C., Thompson, M., Potts, P.J. and Wilson, S., 2012. GeoPT31 – an international proficiency test for analytical geochemistry laboratories – report on round 31/July 2012 (modified river sediment. SdAR-1). International Association of Geoanalysts, unpublished report, 31 p.

Wedepohl, K.H., 1995. The composition of the continental crust. *Geochimica et Cosmochimica Acta*, 59, 1217–1232.

West, A., Firestone, R.B., Kennett, J.P. and Becker, L., 2007. Extraterrestrial markers found at Clovis sites across North America. *EOS Transactions*, 88, abstract PP41A-02.

Wittke, J.H., Weaver, J.C., Bunch, T.E., Kennett, J.P., Kennett, D.J., Moore, A.M.T., Hillman, G.C., Tankersley, K.B., Goodyear, A.C., Moore, C.R., Daniel, I.R., Ray, J.H., Lopinot, N.H., Ferraro, D., Israde-Alcántara, I., Bischoff,

J.L., DeCarli, P.S., Hermes, R.E., Kloosterman, J.B., Revay, Z., Howard, G.A., Kimbel, D.R., Kletetschka, G., Nabelek, L., Lipo, C.P., Sakai, S., West, A. and Firestone, R.B., 2013. Evidence for deposition of 10 million tonnes of impact spherules across four continents 12,800 y ago. *Proceedings of the National Academy of Sciences USA*, 110, E2088–E2097.

Zhu, W., De Leer, E.W.B., Kennedy, M., Kelderman, P. and Alaerts, G.J., 1997. Study of a PLSR model for REE determination by ICP-MS. *Journal of Analytical and Atomic Spectrometry*, 12, 661–665.

Manuscript received 30 Jul., 2015; revised and accepted 6 Apr., 2016